

Improving welding stresses by filler metal and heat control selection in component-related butt joints of high-strength steel

Dirk Schroepfer · Arne Kromm · Thomas Kannengiesser

Received: 11 August 2014 / Accepted: 22 December 2014 / Published online: 18 January 2015
© International Institute of Welding 2015

Abstract The application of high-strength fine-grained structural steels with yield strengths greater than or equal to 690 MPa expands because of present light weight design trends. The requirements regarding the welded components safety increased due to high loading capacity. This determines a sustainable and economic application as well. However, high welding residual stresses could diminish the components safety, especially due to high restraint conditions in component or repair welds. Therefore, this work is concerned with global and local welding stresses, especially crack-critical welding stresses in the HAZ and while root welding due to the restraint conditions. Restraint intensities of real components were analysed and realised with two different weld tests, alongside two different plate dimensions and steel grades. A comparison of the test results showed several significant effects for heat control and restraint intensity regarding restraint forces and local welding stresses. Among these effects, substantial influences were found for the filler metal selection with partially altered results for root and filler beads. Local stresses of weld seam and HAZ were affected differently.

Keywords Residual stresses · MAG welding · Restraint · High-strength steels · Process parameters

Doc. IIW-2532, recommended for publication by Commission II “Arc Welding and Filler Metals”.

D. Schroepfer (✉) · A. Kromm · T. Kannengiesser
BAM Federal Institute for Materials Research and Testing, Berlin,
Germany
e-mail: dirk.schroepfer@bam.de

A. Kromm
e-mail: arne.kromm@bam.de

T. Kannengiesser
e-mail: thomas.kannengiesser@bam.de

1 Introduction

For economic aspects and specific design solutions in, e.g. mobile crane industry, high-strength structural steels are necessary. Furthermore, concerning present light weight design trends, an increasing amount of this steel grades with yield strengths greater than or equal to 690 MPa are applied. High potential weight reductions and cost savings, alongside recent competitions of increasing energy and resource efficiency, emphasise this issue [1]. Among the high requirements of these steels, the achievement of the needed mechanical properties of its welded joints increased as well. Thus, in previous years, steel producers developed various high-strength base and filler metals with a good weldability [2]. Above that, sustainable and economic applications are depending on loading capacity and safety of welded components. Hence, the demands on the component safety are becoming increasingly important. To ensure the mechanical properties as well as sufficient hydrogen effusion and crack resistance, a defined working range regarding heat control and $\Delta t_{8/5}$ -cooling time must be maintained, respectively [3]. Still, high residual stresses in those welds are able to diminish the components safety. In order to determine an adequate heat control before, during and after welding, an enhanced consideration of the interaction between heat control, material and restraint of the surrounding structure is needed. Yet, the recent research activities mainly involved residual stress characteristics in welds of free shrinking laboratory samples [4, 5]. However, several works showed that it is necessary to include heat conduction terms and supporting effects of real component structures as well as filler metal strength in welding stress analysis. Numerous numerical and experimental studies revealed that the reaction stresses in welded structures are highly affected by restraint and component dimensions [6–10]. Particularly, high restraint conditions, occurring while component or repair welding, may cause considerably increased welding stresses

due to superposition of local and global stresses [11]; see Fig. 1.

It was, furthermore, observed that during joining of components, especially crack-critical welding stresses occur at root welding and cooling. Therein, maximum reaction stresses are expected, since the ratio of the load bearing section and arising reaction forces is high; see Fig. 2 [12]. Moreover, after component welds are completed, high welding stresses, appearing in the HAZ, are particularly critical, since the HAZ exhibits a detrimental microstructure [13]. The locally reduced mechanical properties, alongside high tensile stresses, are able to seriously bate the integrity of the welded component. In both cases, appropriate procedures have to be considered to achieve an adequate component safety. Several extensive experimental researches regarding welding of high-strength steels under restraint conditions considered the interaction between heat control and stress build-up [14–16]. It revealed that global and local stresses are substantially influenced by heat control (preheat and interpass temperature, heat input) [14, 15]. Though, basically, the interaction between the magnitude of residual stresses and the superposition of global and local stresses in welded components, among the effect of heat control, is not exceeding quantified. Hence, codes and standards, concerning high-strength steel processing, are leading to an under-utilisation of the high loading capacity of those steels [17, 18].

Within the scope of an AiF-research project (IGF-Nr. 17267 N) experimental analyses were accomplished as well as a component analysis by means of restraint intensity evaluation, in order to quantify the magnitude of welding stresses in high-strength steel components. This work, therefore, presents the enhancement based on [19].

2 Component analysis

A defined restraint in transverse direction during welding and cooling of the specimens can be applied in experiments by clamping them into a test facility;

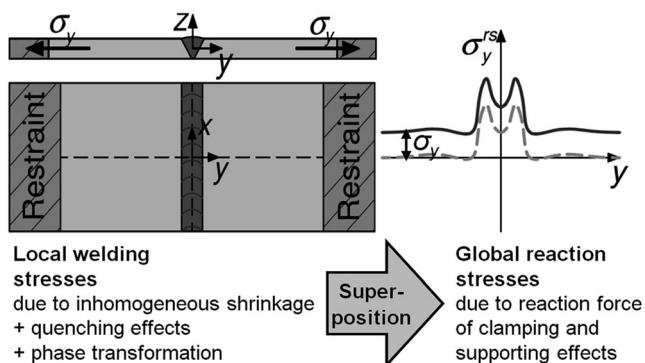


Fig. 1 Superposition of local and global welding stresses due to restraint conditions [8, 14, 19]

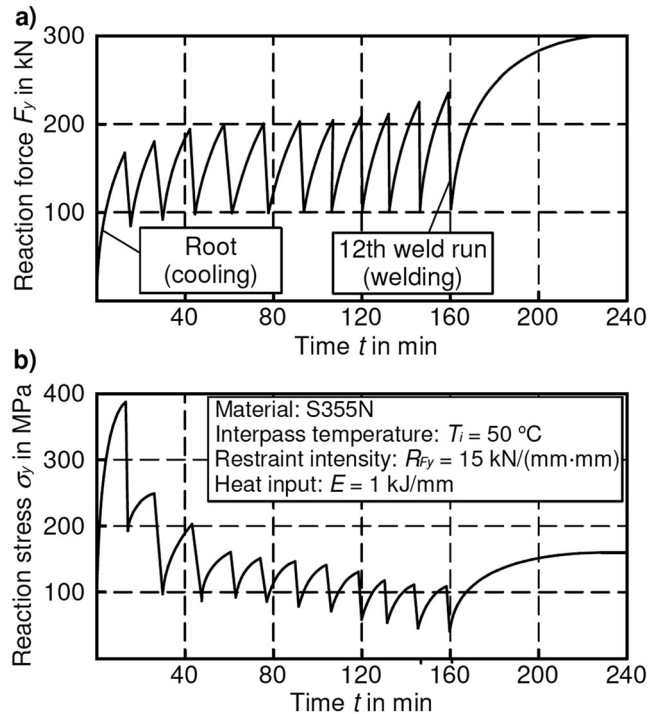


Fig. 2 a Reaction force $F_y(t)$ schematically during welding and cooling due to restraint b corresponding reaction stress $\sigma_y(t)$ schematically according to [12]

see Fig. 1. In order to compare resulting global restraints in different weld constructions, the restraint intensity R_{Fy} was established by Satoh et al. The restraint intensity in weld transverse direction R_{Fy} is the components stiffness towards the weld seam, based on the seam length. It can be estimated for simple butt joints according to [20]; see Eq. 1. In the present study, the transferability of weld test results to real component geometries was analysed. Therefore, a construction detail of a crawler crane was selected as a typical component weld joint, see Fig. 3a. The design of the superstructure was abstracted into a simple FE shell model. Afterwards, the weld seam in the model was loaded by a distributed load of $p=100 \text{ N}/\text{mm}^2$ transverse to weld direction. The FE analysis and the dimensions, as shown in Fig. 3b, allowed determining average deformations Δy_1 and Δy_2 of the weld joint faces due to load and stiffness of the surrounding structure.

With average deformation and total load F_y , the restraint intensity, based on the seam length $L_w=1430 \text{ mm}$, was calculated to $R_{Fy}=1.5 \text{ kN}/(\text{mm}\cdot\text{mm})$; see Eq. 1 [9]:

$$R_{Fy} = \frac{F_y}{L_w(\Delta y_1 + \Delta y_2)}. \quad (1)$$

In the experiments, higher restraint intensities of $R_{Fy}=2 \text{ kN}/(\text{mm}\cdot\text{mm})$ and $3 \text{ kN}/(\text{mm}\cdot\text{mm})$ were applied. The reason was to take it into account that oftentimes the restraint is

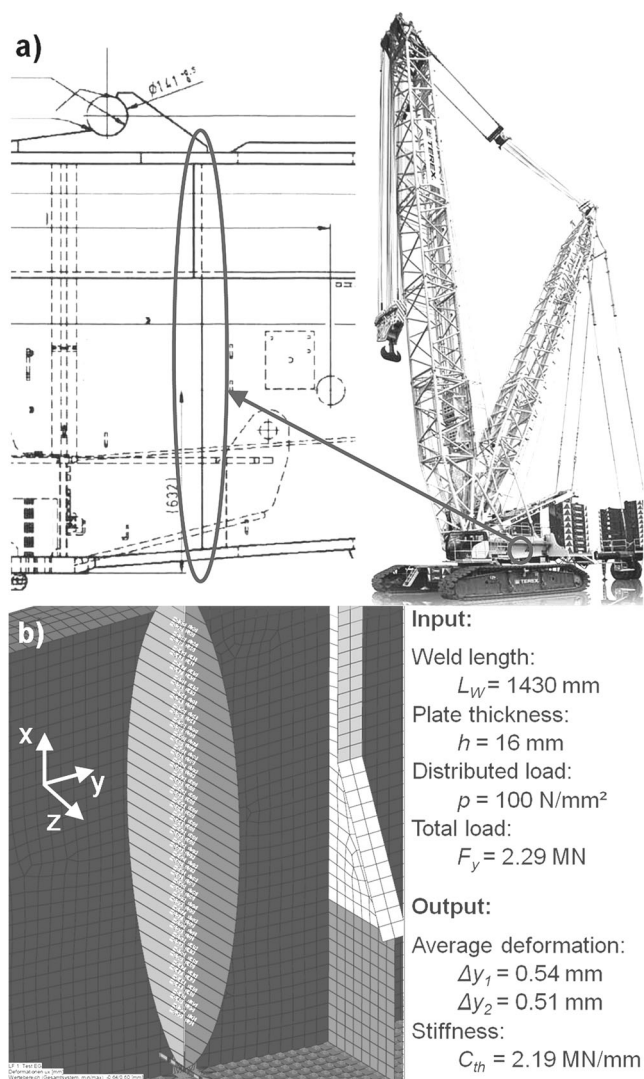


Fig. 3 a Construction detail in a crawler crane (Terex) and b average deformation of the FE-model after transverse loading of the weld seam

more severe, since the weld length is much shorter. Therefore, two different plate dimensions and test facilities were used for the investigations.

3 Experimental

The high-strength quenched and tempered fine-grained structural steels S960QL and S690QL, according to EN 10025-6 [21], with plate thicknesses of $h=8$ and 20 mm were analysed with similar high-strength solid filler wires, according to EN ISO 16834-A [22]. The root of the S960QL plates in 20-mm thickness was welded with the lower strength filler material EN ISO 14341-A–G 46 4 M21 4Si1 [23]. The chemical composition and mechanical properties of the test materials are given in Tables 1 and 2. Automated multilayer MAG-welds were performed in V-groove butt joints. To realise an implementation of the defined restraints in transverse direction during welding and cooling, the specimen plates were clamped into different special in-house developed test facilities; see Fig. 4 [15, 19].

The 8-mm-thick plates were welded in a 0.5-MN-test facility with a restraint intensity of $R_{Fy}=2 \text{ kN}/(\text{mm mm})$; see Fig. 4a [19]. The component weld tests with 20-mm-thick plates were undertaken in the 2-MN-test facility and $R_{Fy}=3 \text{ kN}/(\text{mm mm})$; see Fig. 4b.

The welding process condition and interpass temperature T_i was varied for each plate thickness and steel grade, respectively. The heat input was determined by the actual values of welding current, voltage and speed. The specimen dimensions and welding parameters are shown in Fig. 5. Regarding production relevant process conditions, the $\Delta t_{8/5}$ -cooling times were determined for the specific heat control parameters. The measurement of the $\Delta t_{8/5}$ -cooling times was achieved using a two-colour pyrometer (measuring range 350 to 1300 °C).

During all weld tests, preheat and interpass temperatures were observed using type-K thermocouples attached approx. 10 mm adjacent to the weld seam. In addition, the interpass temperature was monitored with a contact thermocouple on the weld. The local residual stresses in the weld seam area were determined by X-ray diffraction using the $\sin^2\psi$ -method on the top surface of the plates. Since the residual stress analysis for specimens in 8-mm thickness is presented in [19]. Only results of the 20-mm-thick plates are shown in this work.

Table 1 Chemical compositions of test materials (spark emission spectroscopy, Fe balanced)

Element in %	C	Si	Mn	Cr	Mo	Ni	V	Nb	Ti
Base material (a)									
S960QL	0.12	0.22	1.25	0.20	0.58	0.05	0.041	0.015	0.003
S690QL	0.14	0.32	1.15	0.30	0.17	0.07	0.009	0.005	0.010
Filler material (b)									
G 89 6 M21 Mn4Ni2CrMo	0.11	0.71	1.47	0.35	0.62	2.21	0.002	0.001	0.030
G 69 6 M21 Mn4Ni1.5CrMo	0.09	0.43	1.32	0.20	0.55	1.43	0.001	0.001	0.019
G 46 4 M21 4Si1 (c)	0.07	0.82	1.33	0.03	0.01	0.03	0.001	0.002	0.006

(a) EN 10025–6 [21], (b) EN ISO 16834-A [22], (c) root weld of 20 mm S960QL: EN ISO 14341-A [23]

Table 2 Mechanical properties of the test materials

Property	$R_{p0.2}$ in MPa	R_m in MPa	A_5 in %	A_v in J at -40 °C	HV10
Base material (a)					
S960QL	989	1035	17	198	340
S690QL	768	820	19	139	270
Filler material (b)					
G 89 6 M21 Mn4Ni2CrMo	954	1024	15	52	345
G 69 6 M21 Mn4Ni1.5CrMo	733	811	21	88	265
G 46 4 M21 4Si1	530	612	26	81	200

(a) Mechanical testing, (b) producer testing report

4 Results

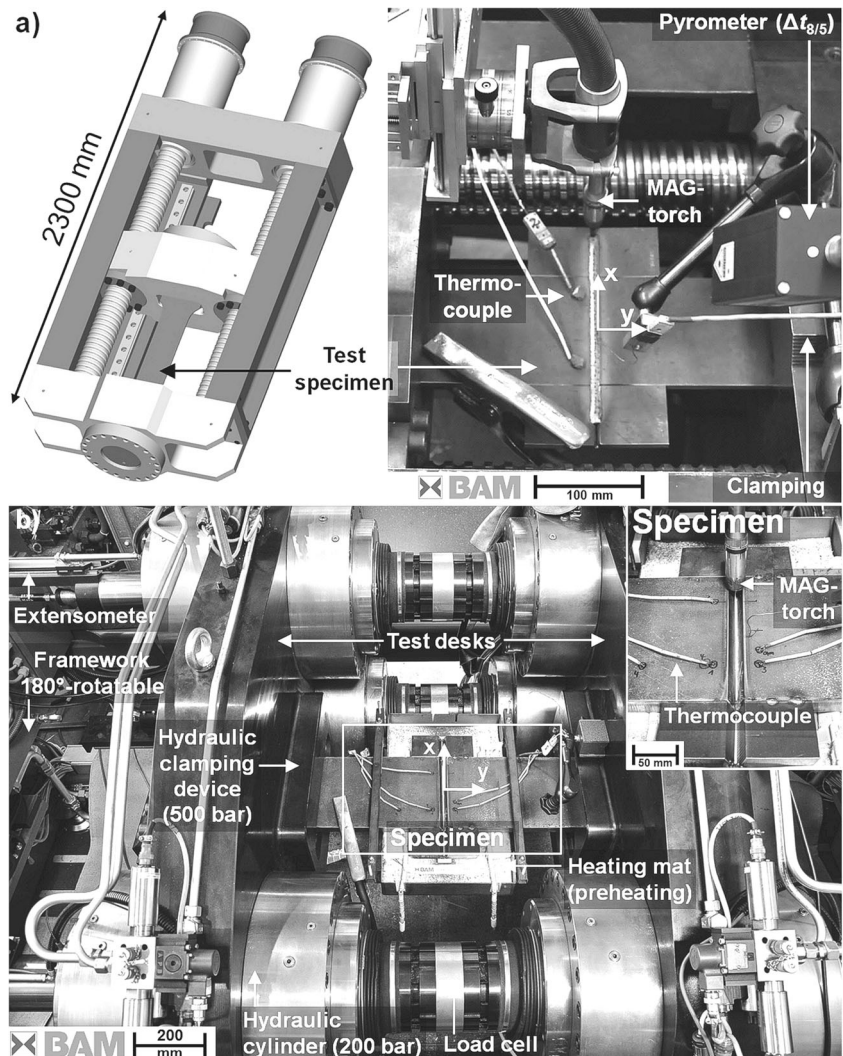
4.1 Cooling times

Figure 6 presents an evaluation of the $\Delta t_{8/5}$ -cooling times determined within the weld tests. It is obvious that the $\Delta t_{8/5}$ -cooling times are significantly affected by interpass temperature T_i , heat input E and plate thickness as well.

4.2 Heat control influence on reaction stresses

This paper discusses primarily the reaction force build-up observed at the weld tests in the 2-MN-test facility, since the results for the 0.5-MN-test facility are presented in [19]. Figure 7a shows the reaction force $F_y(t)$ and temperature $T(t)$ for a 2-MN-weld test with S690QL/G69. At the beginning of the root weld, the reaction force is $F_y = -60$ kN, since

Fig. 4 a 0.5-MN-test facility and b 2-MN-test facility with specimens and weld test equipment



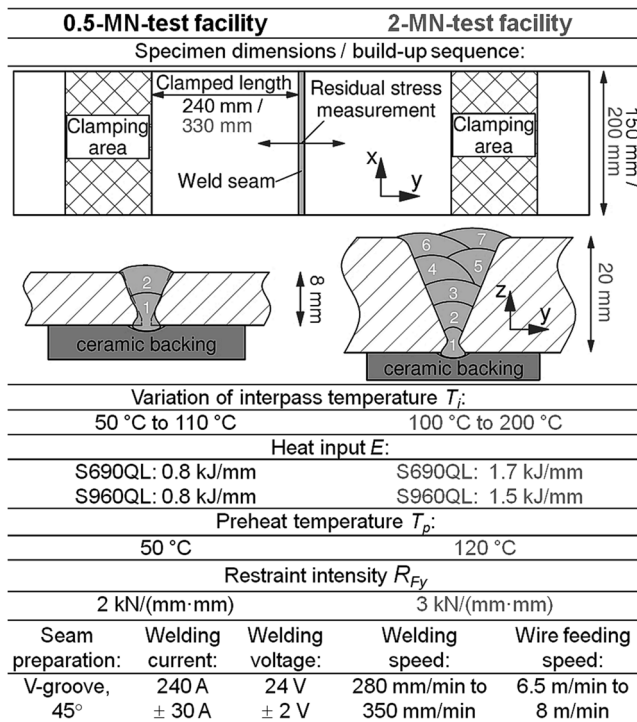


Fig. 5 Specimen dimensions, build-up sequence, restraint intensities and welding parameters for the two plate thicknesses and test facilities

preheating of the tack welded specimen initiates compressive forces. During welding of the root, a force build-up is obvious due to shrinkage of the solidified inserted weld metal, which causes transverse shrinking forces. While the root weld is cooling down to interpass temperature, the reaction force is increasing further with a maximum of $F_y=150$ kN at $T_i=100$ °C. A force reduction is visible while welding the next weld run, since a local heat input combined with stress relief occurs. Subsequent cooling to T_i leads to a new continuous increase of the reaction force and the next weld run, to a force reduction. This force evolution with an increase of the force amplitude was observed for every weld sequence. The amplitude of the force reduction is the result of welding heat input and rises with each run, as well. After completion of the weld

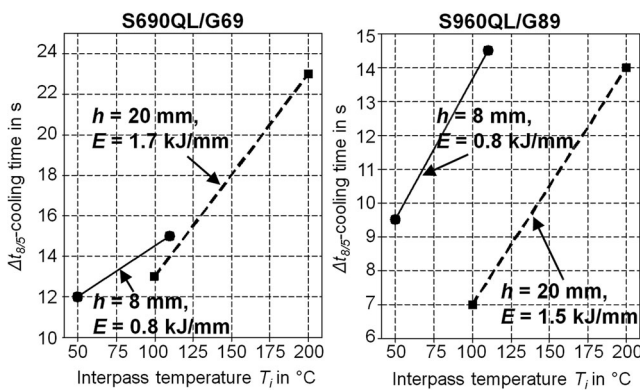


Fig. 6 Evaluation of $\Delta t_{8/5}$ -cooling times versus interpass temperature T_i for two heat input values E and plate thicknesses h

and subsequent cooling to ambient temperature, a maximum reaction force of $F_{y,end}=517$ kN and end reaction stress of $\sigma_{y,end}=129$ MPa based on the plate cross section was measured, respectively. In Fig. 7b, reaction forces $F_y(t)$ for 2-MN-test welds of S690QL/G69 with interpass temperatures of $T_i=100$ °C and $T_i=200$ °C are shown. Whereas the two $F_y(t)$ -graphs exhibit the same tendency, a reduction of total welding time by 55 % using a high interpass temperature ($T_i=200$ °C) is obvious. The comparison of the force amplitudes reveals a lower level for the higher interpass temperature due to shorter cooling cycles. A higher amount of heat remains between each weld run. This leads to a lower decrease of the transverse shrinking forces at each pass. At the last weld run, the reaction force is half as high, compared to the weld with lower interpass temperatures. After cooling to ambient temperature, a remarkable increase of the reaction force for the higher interpass temperature occurs, since the specimen contains a distinct higher heat quantity. The resulting end reaction stress $\sigma_{y,end}$ is about 30 % higher for $T_i=200$ °C.

The reaction force graphs of the 2-MN-weld tests with S960QL/G89 are not shown here, since they revealed the same tendency. It was found that the global reaction stress level is considerably influenced by the heat control and by the restraint intensity; see Fig. 8. High interpass temperatures and high restraint intensities lead to significantly increased global reaction forces after welding and subsequent cooling. This revealed in all butt joints welded under restraint.

4.3 Filler metal influence on reaction stresses

Among the effects of heat control and restraint intensity, significant influences are visible for the filler metal selection in Fig. 8. These end reaction stress differences of about 10 to 20 MPa, displayed in Fig. 8a for the 0.5-MN-weld tests, will be discussed first. Therefore, Fig. 9 shows the reaction force build-up for two 0.5-MN-weld tests with a different base and filler metal selection. The level of the reaction forces for the higher strength steel grades S960QL/G89 is elevated by about $\Delta F_y=15$ kN after root welding.

The reason is a higher reaction force that occurs during welding of the root using higher strength base and filler metals. Apparently, transverse restraint forces are limited by lower high-temperature strengths when welded with lower strength filler metal. While welding of the root, the already inserted weld metal is cooling; see Fig. 9. The highest reactions stresses occur, since the ratio of reaction force to cross section is maximal; see Fig. 2. After welding time $t_w=10$ s, approx. 50 % of the root weld is completed.

At this time, a reaction force maximum appears for both steel grades, shown in the root weld detail of Fig. 9. For the lower strength steel grade S690QL/G69, the reaction force maximum is about 15 kN, and for the S960QL/G89, it is 35 kN. The momentary reaction stress of a weld depends on

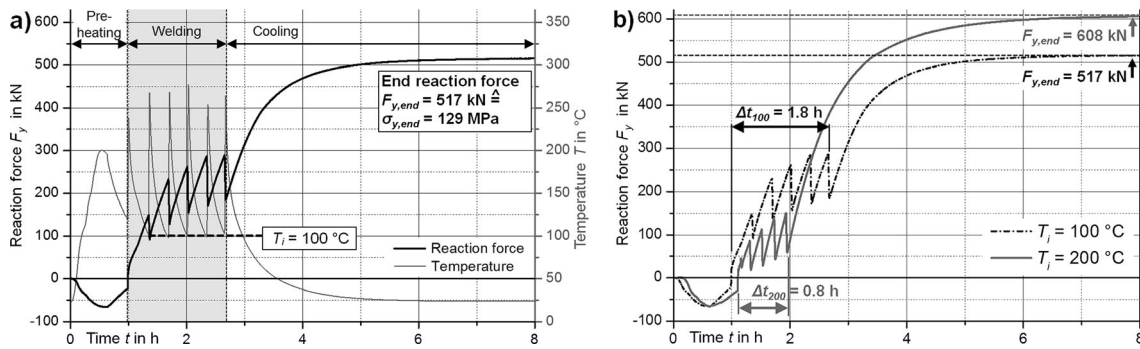


Fig. 7 **a** Reaction force $F_y(t)$ and temperature $T(t)$ for 2-MN-weld test (S690QL, runs: 6, $E=1.7$ kJ/mm, $T_p=120$ °C, $T_i=100$ °C), **b** comparison of reaction forces $F_y(t)$ for two different interpass temperatures T_i (S690QL, 2-MN-test facility, runs: 6, $E=1.7$ kJ/mm, $T_p=120$ °C)

the actual reaction force $F_y(t_w)$ and the height of the inserted weld metal H_w . During a welding process, additionally, the actual weld length $L_w(t_w)$ affects the reaction stress. Thus, the momentary reaction stress can be estimated by

$$\sigma_y(t_w) = \frac{F_y(t_w)}{H_w \cdot L_w(t_w)} \quad (2)$$

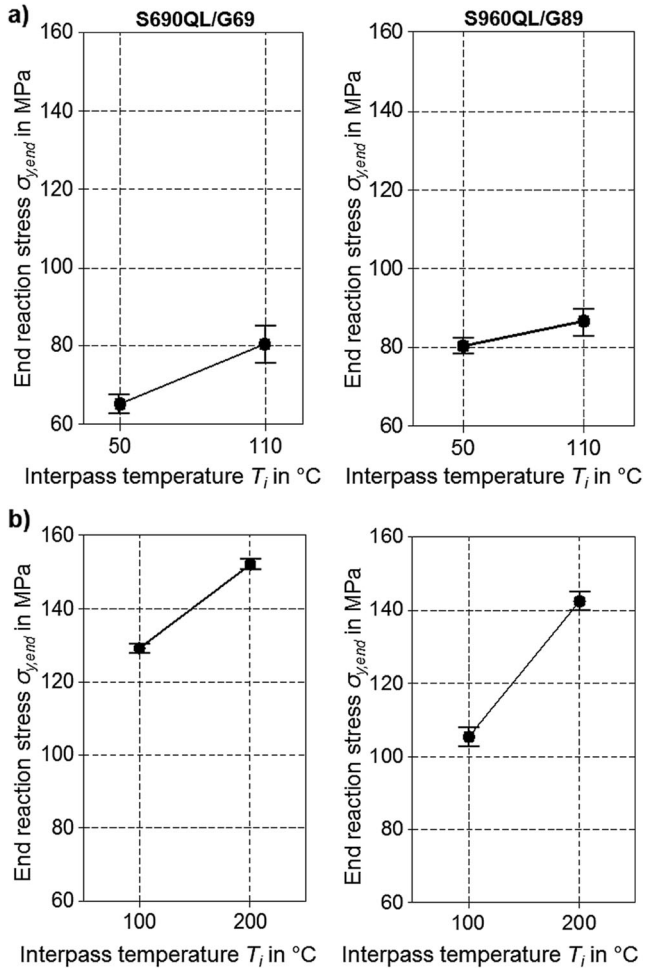


Fig. 8 Reaction stress $\sigma_{y,eng}$ after cooling to ambient temperature versus interpass temperatures T_i for **a** 0.5-MN-test facility 2 kN/(mm mm), 8 mm, and **b** 2-MN-test facility 3 kN/(mm mm), 20 mm (S960QL—filler metal root: G4Si1)

For both weld tests, the height of the root weld is about 4 mm. According to Eq. 2 and Fig. 9, the reaction stress in the welds are approx. $\sigma_y(t_w)=70$ MPa for S690QL/G69 and $\sigma_y(t_w)=120$ MPa for S960QL/G89 when the maximum reaction force occurs. Furthermore, the cooling curves measured with a two-colour pyrometer revealed that after $t_w=10$ s welding time, the beginning of the root welds have cooled down below 600 °C. In addition, by use of the SSDTA (single sensor differential thermal analysis) [24], the transformation temperatures were determined with help of cooling curves. The results of the SSDTA are shown in Fig. 10a. It is, therefore, obvious that phase transformations are present in the weld metal below 600 °C.

Figure 10b shows the comparison of the specific transformation start temperatures and the corresponding phase-specific yield strength at temperature for austenite before the phase transformation starts. It reveals that these specific yield strengths are equal to the maximum reactions stresses. As the lower strength weld metal G69 starts transformation at bainite start temperature ($B_S=600$ °C), basically, into bainite, the G89 transforms into bainite and martensite, in this case. Therein, the transformation temperatures are lower (bainite start

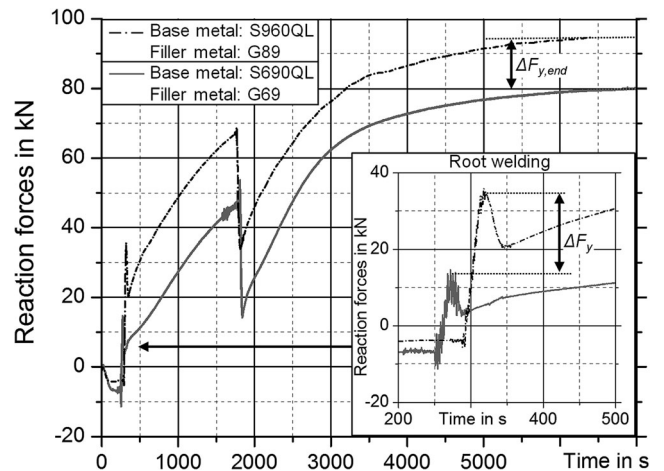


Fig. 9 Comparison of reaction force graphs $F_y(t)$ for two combinations of base and filler material (0.5-MN-test facility, runs: 2, $E=0.8$ kJ/mm, $T_i=50$ °C, $T_p=50$ °C) with detail for the root weld

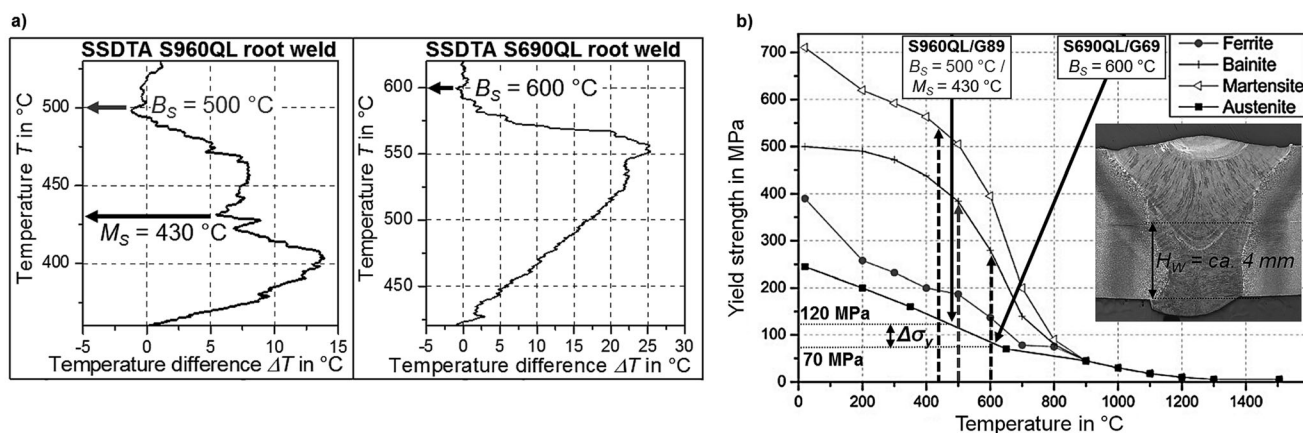


Fig. 10 a SSDTA, root welds of Fig. 9. b Phase-specific yield strength; reference SYSWELD material database [29], max. σ_y and weld metal height for both root welds

temperature $B_S=500$ °C, martensite start temperature $M_S=430$ °C). This affects an austenitic phase with higher yield strength and, therefore, the ability to transfer higher reaction stresses transverse to the root weld. Phase transformation, finally, decreases reaction forces due to volume expansion of the transforming microstructure, in both welds. After phase transformation is completed, the reaction force increases again due to restrained shrinkage; see Fig. 9, since the yield strength of the present microstructure is higher than the reaction stress. The reaction force difference between both steel grades of about $\Delta F_{y,end}=15$ kN due to different phase transformation is still present after welding and cooling of the last weld run. Thus, in the butt joints of the thin walled plates, which were welded with small amounts of runs, higher reaction forces are caused by using higher strength steel grades after welding and cooling.

However, the weld test results of the 20-mm-thick steel plates at the 2-MN-test facility, presented in Fig. 8b, show dissimilar effects. Herein, the reaction stresses are significantly lower for the S960QL/G89 after complete cooling. This is caused by different transformation behaviours of the filler metals, as shown in Fig. 10a. Figure 11 presents the reaction force graphs for both steel grades. Therein, an almost similar reaction force increase while root welding is obvious, since both weld tests were welded with a lower strength root. Though, clear divergences can be observed from the point when the first filler bead is welded. While welding and cooling, the reaction force reduction is rather higher in S960QL/G89. The detail for the third filler bead in Fig. 11 shows a difference of force reduction for both welds, of about $(\Delta F_{y,2}-\Delta F_{y,1})=20$ kN. Since this effect occurs in every weld sequence, the difference of end reaction forces, in case of Fig. 11, is then $\Delta F_y=52$ kN.

The detail of the third filler bead, furthermore, reveals a more severe reaction force build-up after welding, for the lower strength filler metal. Both effects have the same reason, like shown in Fig. 10. Firstly, the lower transformation temperatures of the higher strength filler metal produce higher

compressive forces due to restraint volume expansion in the weld seam, according to common concepts [25, 26]. Secondly, the transformation of G89 into a basically martensitic microstructure leads to a higher compensation of the tensile reaction forces. Since it is a displacive phase transformation, it includes a higher shear component of approx. 24 %. Then, under external load due to restraint, these phase transformation induced shape changes are primarily anisotropic [27, 28]. From this follows a predominant direction of deformation in load direction and, thus, a stronger reduction of transverse restraint forces, in comparison to basically bainitic microstructures of G69. As a result, remarkable welding stress reductions revealed by an application of higher strength filler metals in filler beads.

4.4 Local residual stresses in the weld seam

Primarily, the local transverse residual stresses were analysed. The results of the residual stress determination for the 8-mm-thick plates, welded in the 0.5-MN-test facility, were shown and discussed in [19]. Hence, this work is mainly concerned with the transverse residual stresses of the component-related weld tests. Figure 12 presents the transverse residual stress distributions across the weld seam, for two different interpass temperatures at restrained condition at the centre line ($x=0$ mm) of the specimens. Both graphs show characteristic residual stress distributions for steels, including influences of phase transformation, according to the common concepts [5, 25].

Tensile residual stress maxima occur next to the weld centre line of the last weld run and side peaks at the weld metal next to the fusion line. In each weld run centre, a stress dip occurs due to phase transformation, more or less. A tensile residual stress maximum of 500 MPa (about 50 % of $R_{p0.2}$ of the weld metal) is affected in both weld seams. The tensile residual stress level tends to be increased, especially in the areas near the fusion line, if a higher interpass temperature was used. In order to obtain evidence of the effect

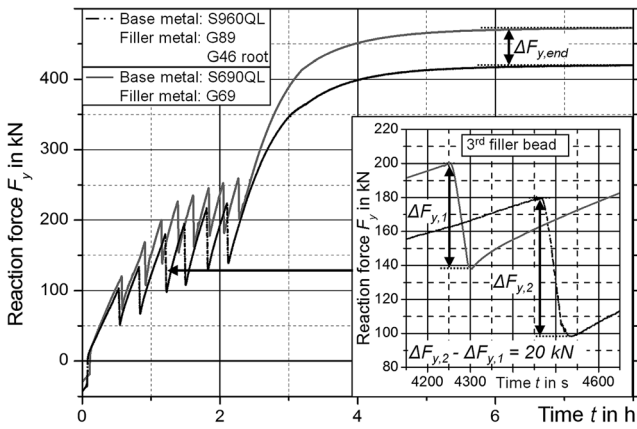


Fig. 11 Comparison of reaction forces $F_y(t)$ for two base and filler metal combinations (2-MN-test facility, runs: 7 and 9, $T_i=100\text{ }^\circ\text{C}$, $T_p=120\text{ }^\circ\text{C}$), detail for third filler bead

significances, overall residual stress levels of the weld seams have to be quantified. The approach of average residual stress is, therefore, introduced in this work by using Eq. 3:

$$\sigma_{y,avg}^{rs}(y_1 \dots y_2) = (1/(y_2 - y_1)) \int_{y_1}^{y_2} \sigma_y^{rs}(y) dy. \quad (3)$$

As a result, average transverse residual stress values $\sigma_{y,avg}^{rs}$ in the weld seam ($y_1=-15\text{ mm}$ to $y_2=15\text{ mm}$) are shown in Fig. 13. It reveals that interpass temperature variation from $T_i=200$ to $100\text{ }^\circ\text{C}$ leads to a significant reduction of the stress level by about 20 %, in S960QL component welds.

One reason for the higher stress level, in case of higher interpass temperature, is the increased temperature level of the joint while the top layer is welded due to shorter cooling cycles. During subsequent cooling to ambient temperature, the more largely heated volume leads to an increased inhomogeneous shrinkage in the weld area. As a result, a higher corresponding tensile stress initiation is involved. Another reason for this effect is the superposition of global reaction stresses [19] that are increased at higher interpass temperature as well; see Fig. 8. Hence, approx. 50 MPa higher average transverse residual stresses $\sigma_{y,avg}^{rs}(-15 \dots +15)$ are initiated in the weld seam by increasing the interpass temperature to $T_i=200\text{ }^\circ\text{C}$ in both steel grades; see Fig. 13. The residual stress magnitudes in the weld seams are tend to be affected almost similarly to global reaction stresses by the heat control.

4.5 Local residual stresses in the HAZ

However, stronger effects were found in the HAZ of the butt joints of the component-related weld tests. In Fig. 14, transverse residual stress distributions across the weld and HAZ of component weld tests with S690QL/G69 for two different interpass temperatures are shown. In both cases, the highest residual stresses next to the maxima of the weld metal are evident in the HAZ. The maximum residual stresses of the

Material	Runs	T_p in $^\circ\text{C}$	T_i in $^\circ\text{C}$	E in kJ/mm	$\Delta t_{8/5}$ in s	Symbol
S960QL/G89	7	120	200	1.5	14	—
			100		7	- - -

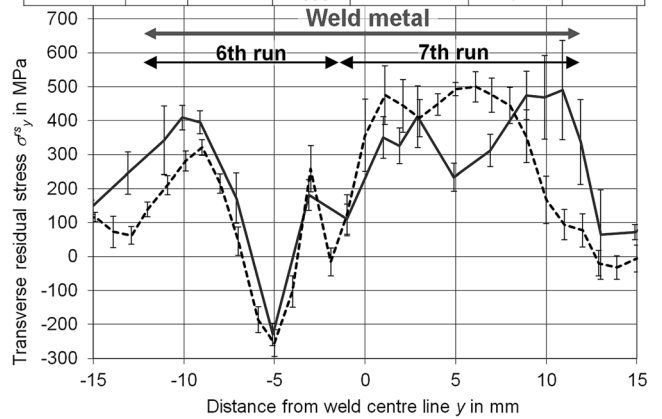


Fig. 12 Transverse residual stress distributions $\sigma_y^{rs}(y)$ for two interpass temperatures T_i in the weld seam of component welds ($x=0\text{ mm}$, S960QL/G89, under restraint)

HAZ, in case of high interpass temperatures, are approx. 300 MPa. This value is equal to the maximum in the weld metal and complies about 40 % of its nominal yield strength. Using a lower interpass temperature of $T_i=100\text{ }^\circ\text{C}$, the residual stress maximum of the HAZ is about 150 MPa, and it is half as high as the maximum in the weld metal. The average transverse residual stresses in the HAZ $\sigma_{y,avg}^{rs}(\pm(15 \dots 30))$, evaluated for both weld joints, give a further indication, see Fig. 15. By increasing interpass temperature from $T_i=100$ to $200\text{ }^\circ\text{C}$, the residual stress level of the HAZ becomes over 100 % higher in the welds of S690QL/G69 due to the additional supporting effect of the clamping. The same tendency is observable for S960QL/G89; see Fig. 15.

Although, it is evident that in higher strength steel grades the residual stress level in the HAZ is significantly lower. This can be explained by the effects due to phase transformation into a different microstructure at lower temperatures; see section 4.3. As a result, the compensation of the tensile reaction

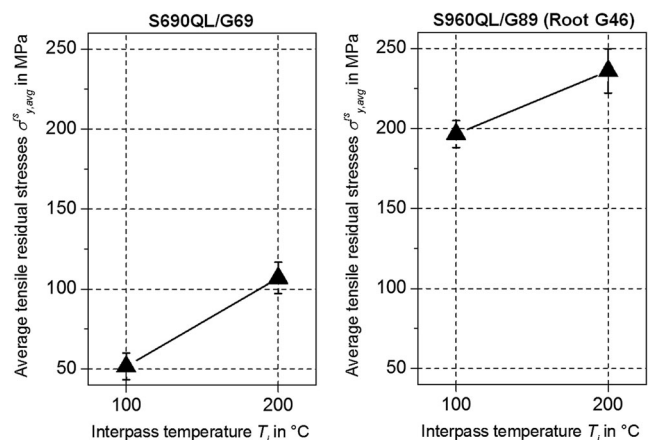


Fig. 13 Average transverse residual stresses in the weld seam $\sigma_{y,avg}^{rs}(-15 \dots +15)$ vs. interpass temperature T_i for both steel grades

forces occurring due to different phase transformation behaviour is higher. This affects a stress reduction in the HAZ, especially while cooling of the cap beads.

In addition to the higher reaction stress levels, the different cooling rates are another subdominant effect on the shown stress increase in the HAZ using higher interpass temperatures. The increase of the $\Delta t_{8/5}$ -cooling times (see Fig. 6) leads in both base and filler metal combinations to about 20 to 30 °C higher transformation start temperatures. This causes a further reduction of compressive forces while welding the cap bead and, therefore, higher tensile stresses, especially in near surface regions of the HAZ.

5 Conclusions

In the present study, the influence of heat control, restraint intensity and filler metal selection on local and global welding stresses in high-strength steel welds were analysed. Plates of 8- and 20-mm thickness were multilayer-MAG-welded under defined restraint in weld transverse direction. The interpass temperature was varied, alongside steel grade and restraint conditions, according to real components. Online measurements allowed an observation of the occurring reaction forces while welding and cooling. The local residual stress determination was performed using X-ray diffraction at weld test specimens. From this work, the following conclusions can be drawn:

1. Primarily, the cooling time determines the intended micro structure and was strongly influenced by the heat control of the specific specimen dimensions. Interpass temperature and plate thickness had a significant effect on $\Delta t_{8/5}$ -cooling time. Additionally, the measured cooling curves

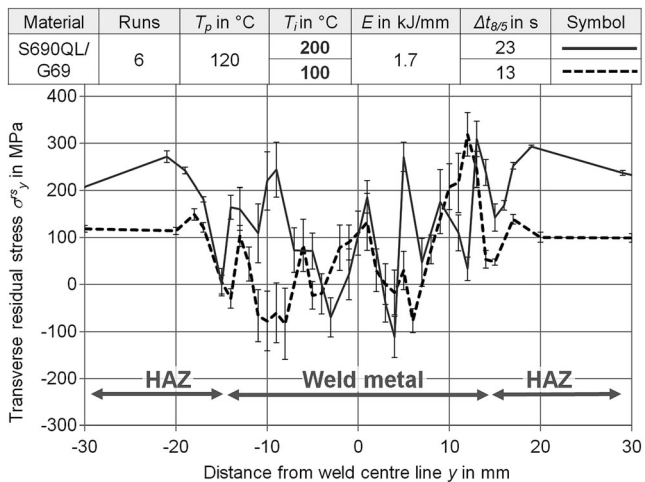


Fig. 14 Transverse residual stress distribution $\sigma_y^s(y)$ for two different interpass temperatures T_i in the weld seam and HAZ of component welds (specimen centre line, $x=0$ mm, S690QL/G69, under restraint)

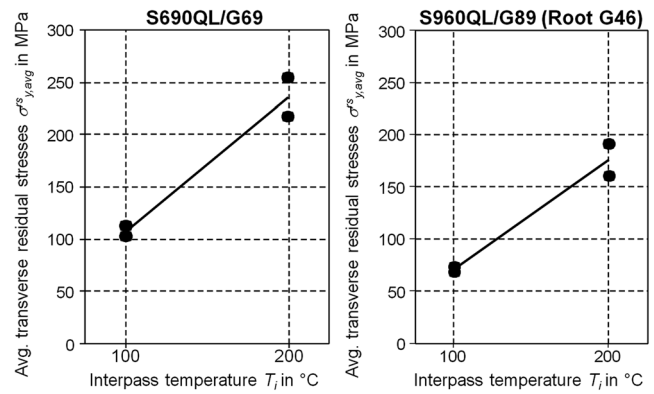


Fig. 15 Average transverse residual stresses in the HAZ $\sigma_{y,avg}^s(\pm(15...30))$ vs. interpass temperature T_i for both steel grades

- gave evidence of phase transformation start temperature, determined by SSDTA.
2. Higher strength filler and base metal combinations lead to higher stresses while welding and cooling of the root because of a higher specific high-temperature strength. From this point of view, lower strength filler metals are recommended for root welding under restraint.
3. The approach of average transverse residual stress was used to quantify influences of heat control under restraint condition on residual stresses. Heat control strongly affects residual stresses in weld transverse direction due to restraint. Higher interpass temperatures lead to significantly increased residual stresses, according to other works [15, 16, 19]. The increase of the restraint intensity from $R_{Fy}=2$ kN/(mm mm) to 3 kN/(mm mm) nearly doubles the restraint stresses.
4. Furthermore, it revealed that the local residual stresses in the crack-critical HAZ are even more affected by heat control. Decreasing interpass temperature from 200 to 100 °C caused a reduction in residual stress magnitude in the HAZ of almost 150 MPa in both steel grades. Contrary to the results of the residual stresses in the weld metal, the residual stress magnitude in the HAZ is nearly 40 % lower in higher strength steel grades S960/G89. The restraint force build-up revealed lower reaction stresses for higher strength filler metals in the filler beads. The reasons are a lower transformation temperature and a different micro structure after phase transformation in higher strength steel grades. Both results in an increased compensation of tensile stresses during phase transformation.
5. Stresses due to welding in the crack-critical root weld and HAZ are decisively affected by heat control and restraint intensity. However, the additional influence of the filler metal selection on both of these stress critical regions in component butt joints has to be taken into account when designing welded components

These analyses of the complex interactions between heat control and stresses due to welding should provide developments of advanced heat control concepts for high-strength structural steel welding and recommendations for existing technical guidelines and standards.

Acknowledgments The studies were funded by the AIF-project IGF-Nr. 17267 N/FOSTA P922. Sincere thanks are given for this support and to the representing companies, actively involved in the project board.

References

- Hulka K, Kern A, Schriever U (2005) Application of niobium in quenched and tempered high-strength steels. In: Materials science forum, Vol. 500–501, pp. 519–526, <http://www.scientific.net/MSF.500-501.519>
- Gliner RE (2011) Welding of advanced high-strength sheet steels. *Weld Int* 25(5):389–396. doi:10.1080/09507116.2011.554234
- Grong Ø (1997) Metallurgical modelling of welding. Institute of materials, ISBN: 9781861250360
- Lachmann C, Krull P, Nitschke-Page T, Wohlfahrt H (1997) Investigations on the cold crack susceptibility of welded S960Q and Ck 45 due to residual stresses. *Int Conf Residual Stress (ICRS-5)* 1:287–295, Sweden
- Nitschke-Pagel T, Wohlfahrt H (1991) The generation of residual stresses due to joining processes. In: Residual stresses—measurement, calculation, evaluation, Hauk V, Hougardy H, Macherauch E (Ed.), pp. 121–133, DGM Informationsgesellschaft mbH, ISBN: 3-88355-169-4
- Wongpanya P, Boellinghaus T, Lothongkum G (2008) Ways to reduce the cold cracking risk in high strength structural steel welds. In: International conference of the international institute of welding, Johannesburg, South Africa
- Boellinghaus T, Kannengiesser T (2003) Effect of filler material selection and shrinkage restraint on stress strain build up in component welds. In: 6th International trends in welding research conference proceedings, Pine mountain, pp. 906–911, ASM International
- Kannengiesser T, Boellinghaus T, Neuhaus M (2006) Effects of the load history on the residual stress distribution in welded components. *Weld World* 50(7–8):11–17. doi:10.1007/BF03266 531
- Boellinghaus T, Kannengiesser T, Neuhaus M (2005) Effects of the structural restraint intensity on the stress strain build up in butt joints. *Math Model Weld Phenom* 7:651–669, 3-901351-99-X
- Satoh K, Terai K, Yamada S, Matsui S, Ohkuma Y, Kinoshita T (1975) Theoretical study on transient restraint stress in multi-pass welding. *Trans Jpn Weld Soc* 6(1):42–52, ISSN: 03859282
- Hirohata M, Itoh Y (2012) Effect of restraint on residual stress generated by butt-welding for thin steel plates. In: 9th German-Japanese Bridge Symposium, Kyoto, Japan, pp. 1–6, <http://hdl.handle.net/2237/18865>
- Kangas P, Sorsa I (1983) Effect of multi-run welding on the deformation and fracture toughness of restraint welded joints. In: Karjalainen LP, Rautioaho R (eds) 3rd Scandinavian symposium in materials science. University of Oulu, Oulu, pp 137–142, 951-42-1547-8
- Schwenk C, Kannengiesser T, Rethmeier M (2009) Restraint conditions and welding residual stresses in self-restrained cold cracking tests. In: Materials research, pp. 766–773
- Rhode M, Kromm A, Kannengiesser T (2013) Residual stresses in multi-layer component welds. In: Trends in welding research: proceedings of the 9th international conference, June 4–8, 2012 Chicago, Illinois, USA, pp. 48–54, ISBN: 1-62708-998-8
- Lausch T, Kannengiesser T, Schmitz-Niederer M (2013) Multi-axial load analysis of thick-walled component welds made of 13CrMoV9-10. *J Mater Process Technol* 213:1234–1240. doi:10.1016/j.jmatprotec.2013.01.008
- Kannengiesser T, Lausch T, Kromm A (2011) Effects of heat control on the stress build-up during high-strength steel welding under defined restraint conditions. In: *Welding in the world*, Vol. 55, Nr. 07, pp. 58–65, Springer, ISSN: 0043–2288
- DIN EN 1011–2 (2001) Welding - Recommendation for welding of metallic materials - Part 2: Arc welding of ferritic steels
- Eurocode 3: Design of steel structures (EN 1993), 2010
- Schroepfer D, Kannengiesser T (2014) Correlating welding reaction stresses and weld process conditions for high-strength steel S960QL. *Weld World* 58(3):423–432. doi:10.1007/s40194 -014-0127-x
- Satoh K, Ueda Y, Matsui S, Natsume M, Terasaki T, Fukuda K, Tsuji M (1977) Japanese studies on structural restraint severity in relation to weld cracking. In: *Welding in the world*, Vol. 15, Nr. 7, pp. 155–189, Springer, ISSN: 0043–2288
- EN 10025–6 (2011) Hot rolled products of structural steels – Part 6: Technical delivery conditions for flat products of high yield strength structural steels in the quenched and tempered conditions
- EN ISO 16834 (2012) Welding consumables – Wire electrodes, wires, rods and deposits for gas shielded arc welding of high strength steels – Classification
- EN ISO 14341 (2011) Welding consumables – Wire electrodes and weld deposits for gas shielded metal arc welding of non alloy and fine grain steels – Classification
- Alexandrov BT, Lippold JC (2007) Single sensor differential thermal analysis of phase transformations and structural changes during welding and postweld heat treatment. In: *Welding in the world*, Vol. 51, Nr. 11–12, pp. 48–59, Springer, DOI: 10.1007/BF03266608%T
- Nitschke-Pagel T, Wohlfahrt H (2002) Residual stresses in welded joints—sources and consequences. *Mater Sci Forum* 404–407:215–226. doi:10.4028/www.scientific.net/MSF.404-407.215
- Dai H, Francis JA, Stone HJ, Bhadeshia HKDH, Withers PJ (2008) Characterizing phase transformations and their effects on ferritic weld residual stresses with X-rays and neutrons. *Metall Mater Trans A* 39(13):3070–3078. doi:10.1007/s11661-008-9616-0
- Bhadeshia HKDH (2004) Developments in martensitic and bainitic steels: role of the shape deformation. In: *Materials science and engineering A*, Elsevier, Vol. 378, Nr. 1–2, pp. 34–39, DOI: 10.1016/j.msea.2003.10.328
- Bhadeshia HKDH (1995) Possible effects of stress on steel weld microstructures. In: Cerjak H (ed) *Mathematical modelling of weld phenomena-II*. Institute of Materials, London, pp 71–115, 978-0-901716-63-7
- Heinze C, Schwenk C, Rethmeier M (2012) Numerical calculation of residual stress development of multi-pass gas metal arc welding. In: *Journal of Constructional Steel Research*, Vol. 72, pp. 12–19, <http://linkinghub.elsevier.com/retrieve/pii/S0143974X11002252>